

Dalton Transactions

Accepted Manuscript



This is an *Accepted Manuscript*, which has been through the Royal Society of Chemistry peer review process and has been accepted for publication.

Accepted Manuscripts are published online shortly after acceptance, before technical editing, formatting and proof reading. Using this free service, authors can make their results available to the community, in citable form, before we publish the edited article. We will replace this *Accepted Manuscript* with the edited and formatted *Advance Article* as soon as it is available.

You can find more information about *Accepted Manuscripts* in the [Information for Authors](#).

Please note that technical editing may introduce minor changes to the text and/or graphics, which may alter content. The journal's standard [Terms & Conditions](#) and the [Ethical guidelines](#) still apply. In no event shall the Royal Society of Chemistry be held responsible for any errors or omissions in this *Accepted Manuscript* or any consequences arising from the use of any information it contains.



Ethylene Glycol-Assisted Coating of Titania on Nanoparticles

Michael Dahl,^a Fernando Castaneda,^a Ji Bong Joo,^a Victor Reyes,^a James Goebel,^a and Yadong Yin^{a*}

Received 00th January 20xx,
Accepted 00th January 20xx

DOI: 10.1039/x0xx00000x

www.rsc.org/

Coating titania shells onto sub-micron sized particles has been widely studied recently, with success mainly limited to objects with sizes above 50 nm. Direct coating on particles below this size has been difficult to attain especially with good control over properties such as thickness and crystallinity. Here we demonstrate titanium-glycolate formed by reacting titanium alkoxide and ethylene glycol is an excellent precursor for coating titania on aqueous nanoparticles. The new coating method is particularly useful for its ability to coat materials lacking strong polymer or ligands which are frequently needed to facilitate typical titania coatings. We demonstrate the effectiveness of the process in coating titania on metal nanoparticles ranging from citrate-stabilized gold and silver spheres to gold nanorods and silver nanoplates, and larger particles such as SiO₂ microspheres and polymer spheres. Further the thickness of these coatings can be tuned from a few nanometers to ~40 nm through sequential coatings. This coating can subsequently be crystallized into TiO₂ through refluxing in water or calcination to obtain crystalline shells. This procedure can be very useful for the production of TiO₂ coatings with tunable thickness and crystallinity as well as for further study on the effect of TiO₂ coatings on nanoparticles.

1. Introduction

The utilization of titanium dioxide (TiO₂, titania) for applications in photocatalysis, solar cells, sensors, etc. has been widely studied in recent years.¹⁻⁴ However, due to the wide band gap of TiO₂, 3.2 eV for anatase and 3.0 eV for rutile,⁵ much work has been done in order to expand the activity to the visible region. One method under current investigation is the addition of metal nanoparticles, such as Au and Ag, in order to utilize their inherent surface plasmon absorption and to improve the separation of photogenerated charge carriers from TiO₂.^{6, 7} Many methods for attachment have been studied, however the sintering of nanoparticles at higher temperatures and the loss of activity under reaction conditions has been of concern. One method for avoiding this activity loss is embedding the particles within the TiO₂ materials.^{7, 8} This method for utilization is promising, however the lack of porosity in the metal oxide shell can greatly decrease the accessibility of reactants to the metal nanoparticle within.⁹ In order to better utilize the properties of such metal-metal oxide composites, core-shell systems have been proposed. Core-shell TiO₂ structures and composites have seen significant research in recent years. Templates such as polystyrene,^{10, 11} silica,¹²⁻¹⁵ iron oxide,^{16, 17} and metal nanoparticles¹⁸⁻²⁴ have all been utilized. These templates have allowed for the placement of the metal nanoparticles within a porous TiO₂ layer for improved accessibility, stability under thermal treatment, and recyclability.^{13, 25}

Unfortunately a wide variety of parameters are needed to

be carefully considered in order to coat this range of materials. Some methods have been established for extending uniform coatings to larger colloids,^{17, 26} however, the uniform coating of TiO₂ onto small metal nanoparticles, i.e. <50 nm diameter, has been difficult to achieve without either significant free TiO₂ particle formation,^{27, 28} or with a well controllable TiO₂ shell thickness.²⁹ Recent progress has been made in the coating of TiO₂ onto both silver nanoplates³⁰ and gold nanorods,^{31, 32} however a comprehensive system is still desirable.

In order to establish a coating method for both small and large particles alike, an ethylene glycol-titanium n-butoxide (EG-TBOT) mixed precursor solution was established. The mixture of titanium alkoxides with EG has been shown previously to produce a chelated complex,^{33, 34} further this particular precursor has been studied for its ability to form highly spherical titania colloids in an acetone solution.³⁵⁻³⁷ Complexation of Ti(IV) with EG yields a titanium glycolate species which is much more stable than the parent titanium alkoxide precursor. This precursor can then undergo a more controlled reaction, catalyzed by the acetone, to produce uniform titanium glycolate microspheres. The role of the acetone as catalyst has been recently uncovered, and it is of note that the purity of the acetone, with respect to water content, is critical to the synthesis of uniform microspheres.³⁶ Once the titanium glycolate products have been formed, crystallization to TiO₂ can be done simply through high temperature calcination.

This study will provide a simple route for depositing a titanium-glycolate coating on several materials including gold and silver spherical nanoparticles (~15-20 nm in diameter), gold nanorods, silver nanoplates, silica microspheres, and resorcinol-formaldehyde polymer microspheres. The effect

^a Department of Chemistry, University of California, Riverside, CA 92521 (USA)

* Corresponding author. E-mail: yadong.yin@ucr.edu

that this coating has on the plasmon absorption of each type of metal nanoparticle will be detailed. Further, the crystallization of the as-coated titanium-glycolate will be studied through refluxing in water as well as by high temperature calcination. Finally, the utilization of hollow TiO₂ shells made by coating a silica template with titanium-glycolate, calcination, and etching will be demonstrated by the degradation of Rhodamine B dye under UV irradiation.

2. Experimental

Titanium-glycolate preparation: Varying volumes of titanium n-butoxide (TBOT, 97%) was added to a vial containing ethylene glycol (EG, 99+%) to a total volume of 20 mL. For example, to produce a 2.5 vol. % precursor solution, 0.500 mL TBOT was mixed with 19.5 mL EG. The resulting solution was then capped and stirred for at least 12 h before use.

Nanoparticle synthesis: Au nanoparticles were synthesized using the Turkevich method³⁸. Briefly 19 μL of $\text{HAuCl}_4 \cdot 3\text{H}_2\text{O}$ (1 g mL^{-1}) was added to 95 mL of water and the solution was heated to reflux. Next trisodium citrate dihydrate (TSC, 99%, 0.034 M, 5 mL) was quickly added to the hot solution. The refluxing was continued for 20 min then the solution was cooled to room temperature and stored. Ag nanoparticles were prepared from reported methods³⁹. In a typical synthesis TSC (13.6 mM, 5 mL) and tannic acid (1.8 μM , 5 mL) were mixed and heated to 60 °C. Separately a solution of AgNO_3 (0.74 mM, 40 mL) was also heated to 60 °C, and upon reaching temperature, the TSC/tannic acid solution was added to it. The mixture was stirred for 3 min, then refluxed for 20 min before cooling and storing in dark conditions at 4 °C. Au nanorods were prepared according to the method from Ye et al. with no modifications⁴⁰. After synthesis, the Au nanorods were concentrated to one-tenth of their original volume and redispersed in water. Ag nanoplates were prepared via a standard citrate reduction without use of polymer surfactant⁴¹. In a typical synthesis TSC (0.075 M, 2 mL) was added to 100 mL of water. To this solution AgNO_3 (0.05 M, 0.200 mL) and H_2O_2 (30 wt. %, 0.120 mL) was added with vigorous stirring. Then fresh, iced NaBH_4 (99%, 0.10 M, 0.200 mL) was added and the reaction was continuously stirred for 30 min, then stored in the dark for future use.

SiO₂ sphere synthesis: SiO₂ microspheres were synthesized using a modified Stöber process. Tetraethyl orthosilicate (TEOS, 99%, 5.16 mL) was mixed with de-ionized water (25.8 mL), ethanol (138 mL) and an aqueous solution of ammonia (26%, 3.72 mL). After stirring for 4 h at room temperature, the colloidal silica particles were separated by centrifugation and washed three times with ethanol, then re-dispersed in 30 mL of ethanol under sonication.

Resorcinol-formaldehyde Sphere Synthesis: Resorcinol-formaldehyde (RF) polymer spheres were made similar to reported procedures^{42, 43}. Water (38 mL), ethanol (16 mL) and aqueous ammonia (28%, 0.200 mL) were mixed for 20 min. To this solution resorcinol (99%, 0.91 M, 2 mL) was added followed by stirring for a few minutes, then a formaldehyde solution (37 wt. %, 0.280 mL) was added, followed by stirring

for 12 h. This solution was then refluxed for 3 h, centrifuged, washed with water three times and stored in 10 mL of water.

Titanium-glycolate coating on SiO₂: To coat SiO₂ microspheres, 3 mL of the above colloid was centrifuged, washed once with acetone, then dispersed in 25 mL of acetone. This dispersion was added to a solution of 50 mL acetone and 0.3 mL water with stirring. To this solution the titanium-glycolate precursor (2.5 vol. % TBOT in EG, 3.75 mL) was slowly injected over the course of 35 min. The solution was then stirred for 30 min, collected by centrifugation, washed once with acetone and twice with ethanol, then stored in ethanol. To produce shells of a thicker coating, this process can be repeated after washing once with acetone.

Titanium-glycolate coating on RF polymer spheres: 2 mL of the above RF suspension were centrifuged, then washed once with acetone, and dispersed in 25 mL of acetone. To this solution water (0.100 mL) was added with stirring, and the titanium-glycolate precursor (1.25 vol. % TBOT in EG, 1.25 mL) was slowly injected over the course of 35 min. The solution was then stirred for 30 min, collected by centrifugation, washed once with acetone and twice with ethanol, then stored in ethanol. To produce shells of a thicker coating, this process can be repeated after washing once with acetone.

Titanium-glycolate coating on nanoparticles: Nanoparticles of gold and silver, as well as silver nanoplates were all coated using a similar method. First 10 mL of the aqueous nanoparticle colloid was concentrated to a volume of 0.100 mL in water. Next a solution of acetone (25 mL) and titanium-glycolate precursor (0.25 vol. % TBOT in EG, 0.020 mL) was prepared. To this solution the nanoparticles were added followed by injection of more titanium-glycolate precursor (0.25 vol. % TBOT in EG, 0.180 mL) over the course of 30 min. The solution was then stirred for 30 min, collected by centrifugation, washed once with acetone and twice with ethanol, then stored in ethanol. To coat gold nanorods, 1 mL of the products of the above synthesis was concentrated to a volume of 0.050 mL. Then the coating procedure follows that of the other nanoparticle systems.

Crystallization of the Titanium-glycolate shell: To crystallize the shell via refluxing the sample is first centrifuged and dispersed into an aqueous sodium fluoride solution (10mM, 25 mL), then refluxed for 1h. Calcination of the sample is done at the desired temperature for 4h at a heating rate of $2.5 \text{ }^\circ\text{C min}^{-1}$.

Characterization: The morphology of each sample was observed by transmission electron microscopy (TEM, Tecnai T12, 120 kV). Surface plasmon resonance absorption spectra were measured by UV-Vis spectrophotometry (HR2000CG-UV-NIR, Ocean Optics). The Raman spectra were measured on a Horiba LabRAM HR confocal imaging system ($\lambda_{\text{ex}} = 532 \text{ nm}$). The crystalline structures were determined by X-ray diffraction (XRD) analyses using Bruker D8 Advance Diffractometer with $\text{Cu K}\alpha$ radiation ($\lambda = 1.5406 \text{ \AA}$). The nitrogen adsorption isotherms were obtained at 77 K using a Quantachrome NOVA 4200e Surface Area and Pore Size Analyzer. The surface area was calculated from the adsorption isotherm using the multi-point BET method in the pressure range of $P/P_0 = 0.05\text{--}0.25$.

Photocatalytic measurements: The catalyst to be tested (5 mg) was dispersed in an aqueous Rhodamine B solution (25 mL, 2.0×10^{-5} M) in a 50 mL quartz cell which was then stirred in the dark for 30 min to ensure adsorption of the dye. The UV lamp (300 W Hg) was used with a 365 nm filter in a commercial reactor system (Xujiang XPA-7). The concentration of RhB was determined by measuring the absorbance on a UV-Vis spectrophotometer (HR2000CG-UV-NIR, Ocean Optics).

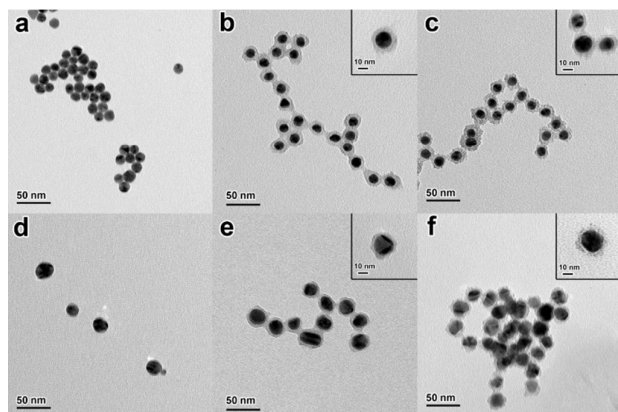
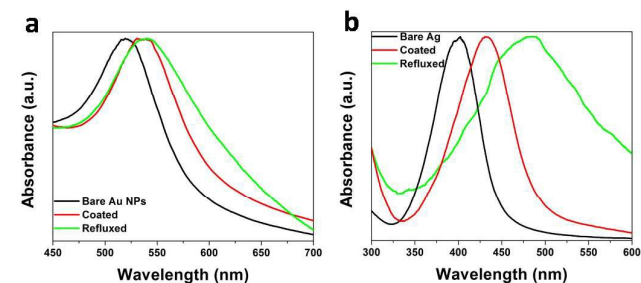


Figure 1. (a-c) TEM images of gold nanoparticles (a) before coating, (b) after coating with titanium glycolate, and (c) after coating and then refluxing in water. (d-f) TEM images of silver nanoparticles (d) before coating, (e) after coating with titanium glycolate, and (f) after coating and then refluxing in water.

3. Results and Discussion

A generalized procedure for the coating of titanium glycolate onto nanoparticles and microspheres has been developed by utilizing a precursor consisting of TBOT in EG. The procedure consists of injecting titanium-glycolate precursor solutions of different concentrations into a colloidal dispersion of the template particles in acetone, with a minor amount of water present. TEM images of gold nanoparticles made by a standard citrate reduction are shown in **Figure 1a** and silver nanoparticles made by reduction using a mixture of trisodium citrate and tannic acid are shown in **Figure 1d**. In order to coat titanium glycolate onto gold and silver nanoparticles, a 0.25 vol. % solution of TBOT in EG was prepared and used. As shown in Figure 1, the coating on nanoparticles of both gold (1b) and silver (1e) has a thickness of approximately 5-8 nm. The as-coated particles were well-dispersed in solution, however upon preparation for TEM, some of the coated particles agglomerated slightly. In order to convert the amorphous coating surrounding the nanoparticles into a crystalline shell, the particles were refluxed in an aqueous solution. Wang et al. demonstrated that amorphous titania materials can be crystallized by aging in water.⁴⁴ This method has additionally been demonstrated to induce the hydrolysis of titanium glycolate microspheres in order to form crystalline TiO₂ as well.^{36, 45} This method of crystallization is very mild and forms small TiO₂ primary particles of predominantly anatase phase with some brookite phase. The

brookite phase can be prevented by the addition of a small amount of an inorganic fluoride source such as NaF or NH₄F.⁴⁴ The TEM images of titanium glycolate coated gold and silver particles after refluxing in water are shown in Figure 1c and 1f, respectively. The images show a marked change in appearance from the smooth amorphous coating to a more granular state, indicating a transition to a more crystalline nature where the shell is made up of small primary TiO₂ particles. It must be noted that after refluxing, these particles do show a more



pronounced tendency towards aggregation.

Figure 2. UV-Vis absorption spectra of (a) gold nanoparticles and (b) silver nanoparticles before coating with titanium glycolate, after coating, and after refluxing in water.

Figure 2 shows the UV-VIS absorption spectra of the gold and silver nanoparticles. Figure 2a shows the spectra of bare gold nanoparticles, coated gold nanoparticles, and coated particles after refluxing. The bare, uncoated gold nanoparticles show a peak near 520 nm, typical of citrate stabilized gold surface plasmon absorption. This peak is then redshifted by approximately 10 nm upon coating by titanium glycolate. It should be noted here that the overall profile of the peak changes little, indicating that the aggregation shown by the TEM results in Figure 1 does not appear in solution. After refluxing, the titanium glycolate coated gold nanoparticles show minimal change in the absorption peak position; however a significant widening of the peak can be attributed to aggregation of the particles. Figure 2b shows the UV-VIS absorption spectra of bare silver nanoparticles, coated silver nanoparticles, and coated particles after refluxing. The bare particles show a peak near 404 nm, typical of silver nanoparticles of the size. Much like with the coating on gold nanoparticles, there is a redshift in the surface plasmon absorption peak, however it is much more pronounced in the case of silver as the peak redshifts ~35 nm to 440 nm. Further the coated particles which appear aggregated by the TEM results do not appear as such in solution as determined by the lack of peak broadening in the spectra. The coated particles after refluxing show both aggregation by the broadening of the peak as well as another significant redshift of ~45 nm to 485 nm.

In order to better demonstrate the utility of this coating methodology, it is necessary to coat titanium glycolate onto particles of different sizes. Other methods frequently reported are optimized for and limited to a narrow range of particle sizes where this method can be used to coat a wide range of

sizes. TEM images demonstrating the extension of this coating method to larger nanoparticles are shown in **Figure 3**. Figures 3a and 3b show TEM images of silver nanoplates of ~40-60 nm in diameter before and after coating, respectively. The coating on the silver nanoplates is less uniform than the coating on the spherical nanoparticles, showing thicknesses between 4-10 nm which may be partially due to the anisotropy of the nanoplates. Figures 3c and 3d show TEM images of gold nanorods before and after coating with titanium glycolate, respectively. The dimensions of the gold nanorods are approximately 60 nm in length and 20 nm in width, with some polydispersity. The coating is approximately 7-10 nm in thickness, and it creates a more uniform coating on individual particles. As with the case of the spherical nanoparticles, both the silver nanoplates and the gold nanorods showed a redshift in the surface plasmon absorption (Figure S1). The bare silver nanoplates show a strong peak at 830 nm which is assigned to the in-plane dipole plasmon resonance. After coating, this peak is redshifted considerably to 907 nm. The gold nanorods show peaks at 514 and 710 nm which are assigned to the transverse and longitudinal plasmon resonance of the rod, respectively. The transverse peak is only redshifted slightly, by ~10 nm whereas the longitudinal peak displays a more pronounced redshift to 752 nm. These two examples depict the ease of coating metal nanoparticles of larger size and of different morphologies without significantly changing the procedure.

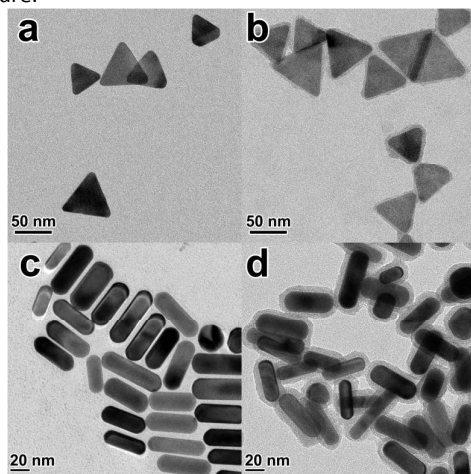


Figure 3. TEM images of silver nanoplates (a) before and (b) after coating with titanium glycolate, and gold nanorods (c) before and (d) after coating with titanium glycolate.

The coating procedure is highly flexible, allowing convenient tuning of the thickness of the titanium glycolate coating by either changing the concentration of templates or by sequential coating. **Figure 4** shows TEM images indicating the difference in the thickness of the titanium glycolate layer on gold nanorods. By changing the amount of gold nanorod templates added into the solution, the thickness of the resulting coating can be changed. Figure 4b shows a thin, non-uniform coating of approximately 1-2 nm which is obtained when the amount of gold nanorods added is at its smallest.

This thickness can be increased by decreasing the amount of gold nanorods added as shown in Figure 4c and 4d. The increase in the thickness of the titanium glycolate layer shows a minimal change on the peak absorption of the surface plasmon resonance (Figure S2). Upon coating with a thin layer, the peak of the longitudinal mode of the gold nanorods redshifts by ~30 nm from 710 to 741 nm; however, the thickest measured coating only further increases the redshift by ~10 nm. This is presumed to indicate that the initial layers deposited form a full coating around the entire particle and subsequent layers of titanium glycolate do not significantly change the dielectric environment surrounding the particle, thus there is little effect on the peak absorption.

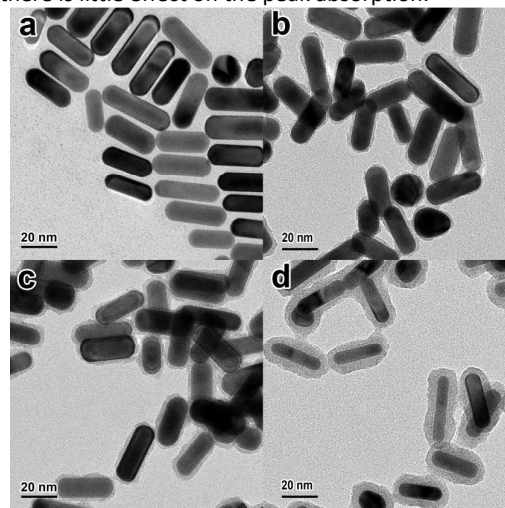


Figure 4. TEM images of different thicknesses of titanium glycolate coating on gold nanorod templates by changing the amount of gold nanorods added to the coating solution.

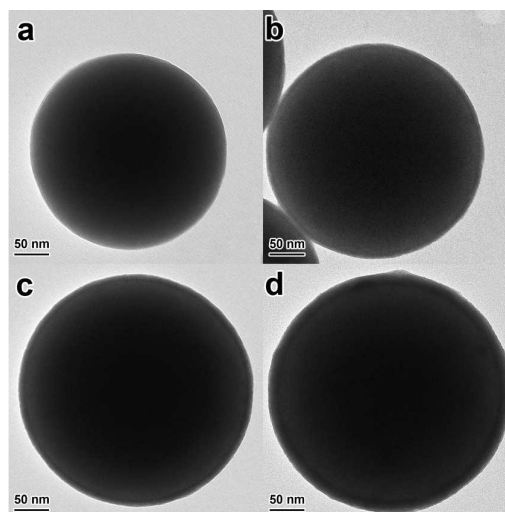


Figure 5. TEM images of (a) bare SiO₂, and (b) single, (c) double, and (d) quadruple coatings of titanium glycolate on SiO₂.

Beyond these metal nanoparticle templates, coating titanium glycolate onto larger templates can be accomplished as well. **Figure 5a** shows the TEM image of an uncoated silica

sphere of approximately 280 nm. Silica microspheres can be easily coated with titanium glycolate simply by changing the concentration of the TBOT:EG precursor to 2.5 vol. % TBOT, as shown in Figure 5b. The coating is highly uniform with a thickness of approximately 7 nm. In addition to adjusting the template/precursor ratio, thicker coatings of titanium glycolate can also be achieved by recoating the templates as shown in Figure 5c and 5d. By collecting the templates after coating, washing to remove the reaction solution, and dispersing in a new coating solution, additional layers of titanium glycolate can be deposited. The limit of this recoating procedure, however, is approximately six coatings or ~40 nm, after which significant self-nucleation occurs. It is our belief that this may be further extended with further modification of the procedure such as decreased concentration of TBOT in the injection solution, though this has not been tested. In addition to silica, resorcinol-formaldehyde (RF) polymer spheres can be coated with titanium glycolate. Figure S3 shows a bare RF polymer sphere of approximately 500 nm in diameter before and after coating, respectively. The coating on RF, as with the case of silica, is highly uniform with a thickness of approximately 7 nm. Lower magnification TEM images of both SiO₂ and RF template coatings show that the coating is uniform across multiple particles and there is little to no self-nucleation (Figure S4).

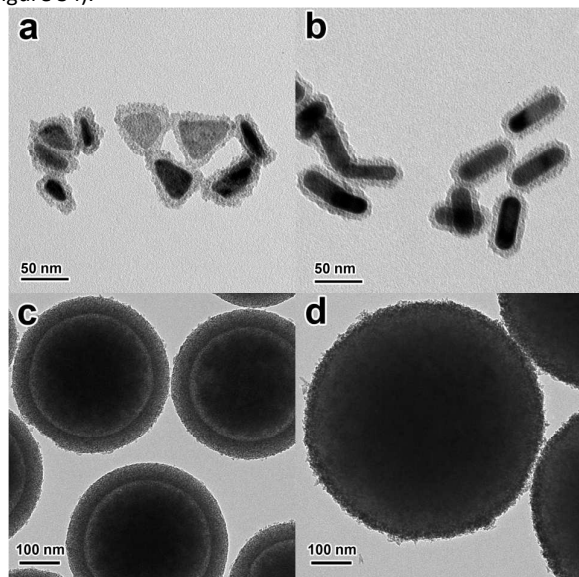


Figure 6. TEM images of titanium glycolate coatings crystallized through refluxing in water on (a) silver nanoplates, (b) gold nanorods, (c) SiO₂ microspheres, and (d) resorcinol-formaldehyde polymer spheres.

Each of the four coated materials shown can also be refluxed in an aqueous solution to crystallize the titanium glycolate to TiO₂. **Figure 6** shows TEM images of each of these particles after refluxing. Similar to the coating on gold and silver nanoparticles discussed above, the titanium glycolate becomes noticeably granulated, indicating a change from an amorphous coating to crystalline. As mentioned above, the

crystallization of TiO₂ in an aqueous solution forms a mixture of anatase and brookite phases; however the brookite phase can be inhibited by the addition of fluoride. It should be noted that in the case of refluxing titanium glycolate coated SiO₂ microspheres, the fluoride source (NaF) yields a basic environment which at elevated temperature induces the dissolution of the SiO₂ template, as seen in Figure 6c. The crystallization of these materials can be monitored by Raman spectroscopy, as shown in **Figure 7**. This method is preferable compared to X-ray diffraction (XRD) because when the templates are still present, the contribution to the signal for XRD by the template is significantly greater than that of the crystalline TiO₂ due to both its relatively low percent composition as well as its low crystallinity. Raman spectroscopy on the other hand can better measure the surface of the core-shell composite where TiO₂ is primarily located. **Figure 7** shows the Raman spectra of refluxed SiO₂@titanium glycolate, refluxed Au nanorods@titanium glycolate, and titanium glycolate particles without a template or refluxing. Both spectra of the refluxed core-shell particles show peaks indicative of anatase phase TiO₂ at 142, 397, 510, and 639 cm⁻¹ which can be attributed to the E_g, B_{1g}, A_{1g}, and E_g symmetries respectively.⁴⁶ Due to the use of fluoride during the refluxing process, there is no indication of brookite phase in the Raman spectra. The bare, non-refluxed titanium glycolate particles show no discernable peaks, typical of its amorphous nature.⁴⁷

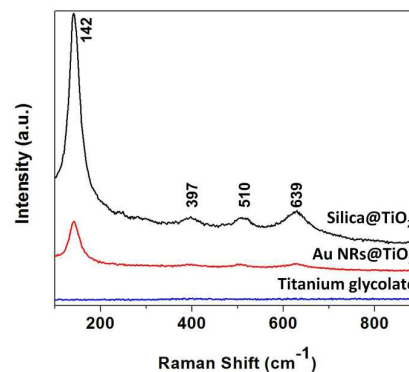


Figure 7. Raman spectra of titanium glycolate coatings on gold nanorods and SiO₂ microspheres after refluxing, indicating conversion to anatase crystal phase. $\lambda_{\text{ex}} = 532 \text{ nm}$.

In addition to crystallization through refluxing in an aqueous solution, the titanium glycolate coating can also be directly crystallized to TiO₂ through calcination.^{37, 48} This is best exemplified using SiO₂@titanium glycolate since the silica core can easily be removed via etching with sodium hydroxide after calcination to yield a hollow TiO₂ shell. **Figure 8a-d** shows TEM images of hollow TiO₂ shells which were prepared by calcination of the SiO₂@titanium glycolate composite followed by etching to remove the SiO₂ core. It is apparent from the images that the morphology of the resulting TiO₂ shell is quite different than the crystalline shells produced by refluxing in an aqueous solution. When the samples are calcined at 400 °C, the hollow TiO₂ shells appear to consist of smaller primary

particles connected to form a shell. It is of note here that the shells appear to contract in size after calcination which is consistent with contraction seen in titanium glycolate microspheres.³⁷ As the calcination temperature is increased, the shells become much denser and appear to consist of larger crystal domains. As these crystal domains grow larger, the shells have a greater tendency to break apart into smaller crystals (Figure S6). X-ray diffractograms of the hollow TiO₂ shells, as shown in **Figure 8e**, show peaks at $2\theta = 25.3, 36.9, 37.8, 38.5, 48.0, 53.8$ and 54.9° which are attributed to the (101), (103), (004), (112), (200), (105) and (211) planes of the anatase TiO₂ crystal lattice. Further the sharpness of the peaks indicates that the samples are of a high degree of crystallinity. The retention of anatase phase and inhibition of rutile formation may be explained by the presence of SiO₂. In our previous studies we have seen both an inhibition of TiO₂ crystal grain growth by SiO₂ as well as the inhibition of transition to the rutile crystalline phase,^{49, 50} even as the individual grains grow larger than the typical size where transition begins of ~ 14 nm.⁵¹ It is presumed that here, although SiO₂ is present in the core and not as a shell, the penetration of SiO₂ oligomers from the surface of the core into the titanium glycolate shell layer successfully inhibits transition to the rutile phase, even as the grain size grows larger than 14 nm.

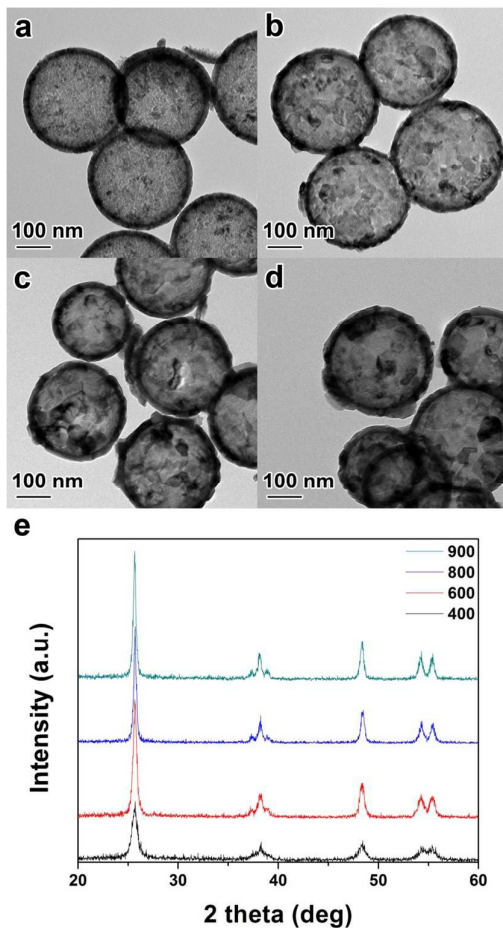


Figure 8. TEM images of hollow TiO₂ shells obtained by calcination of SiO₂@titanium glycolate, followed by base etching. Samples shown were calcined at (a) 400, (b) 600, (c) 800, and (d) 900 °C. (e) XRD diffractograms of hollow TiO₂ shells obtained by calcination and etching of SiO₂@titanium glycolate indicating conversion to anatase crystal phase.

From the XRD data, the increase in the sharpness of the peaks indicates an increase in the size of the crystal grains of the TiO₂ hollow shells which can be approximated using the Scherrer equation. **Figure 9a** summarizes the increase in the calculated grain size versus the calcination temperature. The SiO₂@titanium glycolate samples calcined as low as 400 °C still show a remarkably high degree of crystallinity, with grain sizes of approximately 11 nm. Once calcined above 500 °C, the 14 nm threshold is passed while the TiO₂ shells produced are still pure anatase phase. Calcination at 600 °C results in calculated grain sizes of ~ 18 nm, and once the SiO₂@titanium glycolate samples have been calcined to 800 °C, the grain size plateaus at ~ 23 nm. It is interesting to note that as the calcination temperature is increased to 900 °C, the grain size does not change appreciably. This is attributed to the fact that above 800 °C, the shell morphology significantly degrades and the shells break apart. As this occurs it can then be hypothesized that the broken shells do not fuse together and as such do not grow further. The surface areas of the hollow TiO₂ shells after calcination were measured using the multi-point Brunauer-Emmett-Joyner (BET) method from the adsorption branch in the relative pressure range of 0.05–0.25, which is summarized in **Figure 9b**. The typical isotherm shows a type IV isotherm with hysteresis indicating presence of mesopores (Figure S7).

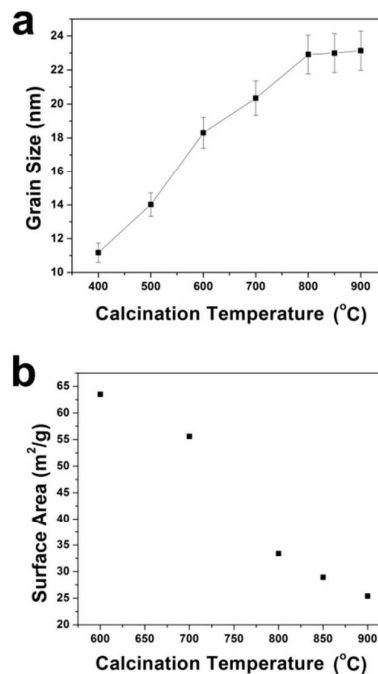


Figure 9. (a) Summary of grain sizes of crystalline TiO₂ hollow shells as calculated by the Scherrer equation versus the calcination temperature. (b) Summary of the surface areas measured by the multi point BET method of hollow TiO₂ versus the calcination temperature.

Since the hollow TiO_2 shells display such a high degree of crystallinity, the application of the hollow shells towards photocatalysis becomes of interest. The photocatalytic activity of the hollow TiO_2 shells produced after calcination and etching of the SiO_2 @titanium glycolate composites was demonstrated by measuring the degradation of Rhodamine B (RhB) dye under UV irradiation over time. **Figure 10a** displays the change in concentration of the dye versus time as measured by the decrease in absorption of the characteristic RhB peak at 533 nm. The blank sample without catalyst shows minimal degradation over the one hour time period measured whereas all hollow TiO_2 samples showed at least 90% degradation in the same timeframe. The best sample was the hollow TiO_2 shells produced after calcination at 700 °C, which showed a photocatalytic activity comparable to P25 TiO_2 . This activity is attributed to the high degree of crystallinity of the sample, which showed a grain size of ~ 20 nm. The samples calcined at higher temperatures were lower in activity even though, by calculation from the XRD data, the grain sizes of both were ~ 23 nm. The difference in the photocatalytic activity of these samples may be attributed to the fact that the sample calcined at 700 °C has a surface area of approximately $56 \text{ m}^2 \text{ g}^{-1}$ where the samples calcined at 800 and 900 °C have surface areas of 33 and $25 \text{ m}^2 \text{ g}^{-1}$, respectively (Figure 9b). In addition to the surface area difference, the sample calcined at 700 °C retains the hollow shell morphology which allows it to be more easily dispersed in the photocatalysis reaction solution. The sample calcined at 600 °C also shows a higher photocatalytic activity despite a lower grain size than the samples calcined at 800 and 900 °C, which indicates that there is a midpoint between the benefits of an increased grain size and surface area.⁴⁹ Figure 10b shows the linear relationship of plotting $\ln(C/C_0)$ versus reaction time while irradiated, indicating first order reaction kinetics. Each sample tested matches first order kinetics with R^2 values of at least 0.99. Using the formula $\ln(C/C_0) = -kt$, we can determine the apparent rate constant, k . From this data it is noticed that the sample calcined at 700 °C and P25 are quite similar in activity with k values of $\sim 0.086 \text{ min}^{-1}$ for each. As expected the k values then decrease to 0.046, 0.038, and 0.035 min^{-1} for the samples calcined at 600, 800, and 900 °C, respectively. The reaction kinetics further show that the sample calcined at 700 °C has an optimal grain size, surface area, and morphology which allow it to have a photocatalytic activity close to that of P25 TiO_2 .

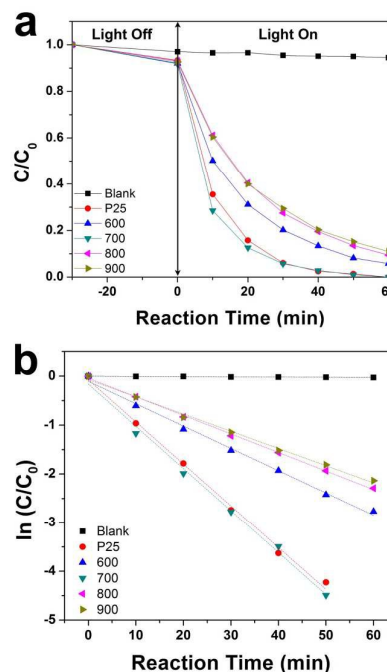


Figure 10. (a) Photocatalytic degradation of Rhodamine B dye by the prepared hollow TiO_2 shells under UV irradiation with a 366 nm filter. (b) Apparent reaction rate versus UV irradiation time for the same catalysts.

4. Conclusions

We have developed a method which allows for easy coating of a titanium glycolate layer onto nanomaterials covering a wide range of sizes, from nanoparticles to microspheres, by simply changing the concentration of the titanium alkoxide in the precursor solution. The coatings can be controlled in thickness from only a few nanometers to approximately 20 nm in a single step, and up to 40 nm with multiple times of coating. The titanium glycolate coating can then be crystallized to anatase TiO_2 by either refluxing in an aqueous solution or by calcination. Calcination yields larger grain size anatase TiO_2 which, after removal of the SiO_2 template, can be converted to hollow TiO_2 shells. By controlling the calcination temperature, it has been possible to optimize the catalyst and achieve photocatalytic activity comparable to commercial P25 TiO_2 . With the main merits of its simplicity and generality, this method may be an alternative method to the conventional sol-gel process for the synthesis of metal@ TiO_2 composite materials which can be used for applications in sensors, photovoltaic cells, and catalysis.

Acknowledgements

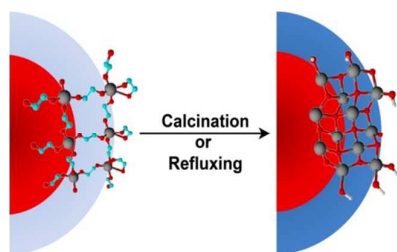
Y.Y. is grateful for the support from the U.S. Department of Energy, Office of Science, Basic Energy Sciences, Chemical Sciences, Geosciences, & Biosciences (CSGB) Division, under

Award No. DE-SC0002247, and he is a member of the Center for Catalysis at the University of California, Riverside.

Notes and references

1. B. O'Regan and M. Gratzel, *Nature*, 1991, **353**, 737-740.
2. X. Chen and S. S. Mao, *Chem. Rev.*, 2007, **107**, 2891-2959.
3. D. Chen and R. A. Caruso, *Adv. Funct. Mater.*, 2013, **23**, 1356-1374.
4. M. Dahl, Y. Liu and Y. Yin, *Chem. Rev.*, 2014, **114**, 9853-9889.
5. D. Hanaor and C. Sorrell, *J. Mater. Sci.*, 2011, **46**, 855-874.
6. A. Furube, L. Du, K. Hara, R. Katoh and M. Tachiya, *J. Am. Chem. Soc.*, 2007, **129**, 14852-14853.
7. K. Awazu, M. Fujimaki, C. Rockstuhl, J. Tominaga, H. Murakami, Y. Ohki, N. Yoshida and T. Watanabe, *J. Am. Chem. Soc.*, 2008, **130**, 1676-1680.
8. J. He, I. Ichinose, T. Kunitake, A. Nakao, Y. Shiraishi and N. Toshima, *J. Am. Chem. Soc.*, 2003, **125**, 11034-11040.
9. F. Zaera, *Chem. Soc. Rev.*, 2013, **42**, 2746-2762.
10. Z. Zhong, Y. Yin, B. Gates and Y. Xia, *Adv. Mater.*, 2000, **12**, 206-209.
11. G. K. Li and Z. C. Zhang, *Mater. Lett.*, 2004, **58**, 2768-2771.
12. M. Ye, Q. Zhang, Y. Hu, J. Ge, Z. Lu, L. He, Z. Chen and Y. Yin, *Chemistry - A European Journal*, 2010, **16**, 6243-6250.
13. I. Lee, J. B. Joo, Y. Yin and F. Zaera, *Angew. Chem., Int. Ed.*, 2011, **50**, 10208-10211.
14. J. B. Joo, Q. Zhang, I. Lee, M. Dahl, F. Zaera and Y. Yin, *Adv. Funct. Mater.*, 2012, **22**, 166-174.
15. W. Li and D. Zhao, *Adv. Mater.*, 2013, **25**, 142-149.
16. X. W. Lou and L. A. Archer, *Adv. Mater.*, 2008, **20**, 1853-1858.
17. W. Li, J. Yang, Z. Wu, J. Wang, B. Li, S. Feng, Y. Deng, F. Zhang and D. Zhao, *J. Am. Chem. Soc.*, 2012, **134**, 11864-11867.
18. I. Pastoriza-Santos, D. S. Koktysh, A. A. Mamedov, M. Giersig, N. A. Kotov and L. M. Liz-Marzán, *Langmuir*, 2000, **16**, 2731-2735.
19. K. S. Mayya, D. I. Gittins and F. Caruso, *Chem. Mater.*, 2001, **13**, 3833-3836.
20. D. S. Koktysh, X. Liang, B. G. Yun, I. Pastoriza-Santos, R. L. Matts, M. Giersig, C. Serra-Rodríguez, L. M. Liz-Marzán and N. A. Kotov, *Adv. Funct. Mater.*, 2002, **12**, 255-265.
21. L. M. Liz-Marzán and P. Mulvaney, *J. Phys. Chem. B*, 2003, **107**, 7312-7326.
22. R. T. Tom, A. S. Nair, N. Singh, M. Aslam, C. L. Nagendra, R. Philip, K. Vijayamohanan and T. Pradeep, *Langmuir*, 2003, **19**, 3439-3445.
23. Y. Chen, B. Zhu, M. Yao, S. Wang and S. Zhang, *Catal. Commun.*, 2010, **11**, 1003-1007.
24. J. Goebel, J. B. Joo, M. Dahl and Y. Yin, *Catal. Today*, 2014, **225**, 90-95.
25. Q. Zhang, D. Q. Lima, I. Lee, F. Zaera, M. Chi and Y. Yin, *Angew. Chem.*, 2011, **123**, 7226-7230.
26. A. F. Demirörs, A. van Blaaderen and A. Imhof, *Langmuir*, 2010, **26**, 9297-9303.
27. T. Hirakawa and P. V. Kamat, *J. Am. Chem. Soc.*, 2005, **127**, 3928-3934.
28. J. Qi, X. Dang, P. T. Hammond and A. M. Belcher, *ACS Nano*, 2011, **5**, 7108-7116.
29. N. Zhang, S. Liu, X. Fu and Y.-J. Xu, *J. Phys. Chem. C*, 2011, **115**, 9136-9145.
30. P. Du, Y. Cao, D. Li, Z. Liu, X. Kong and Z. Sun, *RSC Advances*, 2013, **3**, 6016-6021.
31. S. Mubeen, J. Lee, N. Singh, S. Kramer, G. D. Stucky and M. Moskovits, *Nat. Nanotechnol.*, 2013, **8**, 247-251.
32. F. Wang, C. Li, H. Chen, R. Jiang, L.-D. Sun, Q. Li, J. Wang, J. C. Yu and C.-H. Yan, *J. Am. Chem. Soc.*, 2013, **135**, 5588-5601.
33. R. E. Reeves and L. W. Mazzeno, *J. Am. Chem. Soc.*, 1954, **76**, 2533-2536.
34. D. Wang, R. Yu, N. Kumada and N. Kinomura, *Chem. Mater.*, 1999, **11**, 2008-2012.
35. M. Pal, J. García Serrano, P. Santiago and U. Pal, *J. Phys. Chem. C*, 2006, **111**, 96-102.
36. X. Yang, H. Fu, A. Yu and X. Jiang, *J. Colloid Interface Sci.*, 2012, **387**, 74-83.
37. X. Jiang, T. Herricks and Y. Xia, *Adv. Mater.*, 2003, **15**, 1205-1209.
38. J. Turkevich, P. C. Stevenson and J. Hillier, *Discuss. Faraday Soc.*, 1951, **11**, 55-75.
39. T. Dadosh, *Mater. Lett.*, 2009, **63**, 2236-2238.
40. X. Ye, C. Zheng, J. Chen, Y. Gao and C. B. Murray, *Nano Lett.*, 2013, **13**, 765-771.
41. Q. Zhang, N. Li, J. Goebel, Z. Lu and Y. Yin, *J. Am. Chem. Soc.*, 2011, **133**, 18931-18939.
42. J. Liu, S. Z. Qiao, H. Liu, J. Chen, A. Orpe, D. Zhao and G. Q. Lu, *Angew. Chem., Int. Ed.*, 2011, **50**, 5947-5951.
43. N. Li, Q. Zhang, J. Liu, J. Joo, A. Lee, Y. Gan and Y. Yin, *Chem. Commun.*, 2013, **49**, 5135-5137.
44. D. Wang, L. Liu, F. Zhang, K. Tao, E. Pippel and K. Domen, *Nano Lett.*, 2011, **11**, 3649-3655.
45. L.-S. Zhong, J.-S. Hu, L.-J. Wan and W.-G. Song, *Chem. Commun.*, 2008, 1184-1186.
46. T. Ohsaka, F. Izumi and Y. Fujiki, *J. Raman Spectrosc.*, 1978, **7**, 321-324.
47. M. Pal, J. García Serrano, P. Santiago and U. Pal, *J. Phys. Chem. C*, 2007, **111**, 96-102.
48. X. Jiang, Y. Wang, T. Herricks and Y. Xia, *J. Mater. Chem.*, 2004, **14**, 695-703.
49. M. Dahl, S. Dang, J. Bong Joo, Q. Zhang and Y. Yin, *CrystEngComm*, 2012, **14**, 7680-7685.
50. J. B. Joo, Q. Zhang, M. Dahl, I. Lee, J. Goebel, F. Zaera and Y. Yin, *Energy Environ. Sci.*, 2012, **5**, 6321-6327.
51. H. Zhang and J. F. Banfield, *J. Mater. Chem.*, 1998, **8**, 2073-2076.

TOC Figure



Ethylene glycol can complex with titanium alkoxide to yield a chelated and stabilized titanium glycolate species that can be used as an excellent precursor for coating nanoscale colloidal objects. The titanium glycolate coating can be converted to crystalline TiO_2 either through high temperature calcination or refluxing in water, yielding core@shell TiO_2 composites or hollow TiO_2 shells.